2474 *Macromolecules* **2010**, *43*, 2474–2483
DOI: 10.1021/ma902227g

Macromolecules
ARTICLE

Aqueous Solution Properties of the Acid-Labile Thermoresponsive Poly(meth)acrylamides with Pendent Cyclic Orthoester Groups

Fu-Sheng Du, Xiao-Nan Huang, Guang-Tao Chen, Shrong-Shi Lin, Dehai Liang, and Zi-Chen Li*

Beijing National Laboratory for Molecular Sciences, Key Laboratory of Polymer Chemistry and Physics of Ministry of Education, College of Chemistry & Molecular Engineering, Peking University, Beijing 100871, P. R. China

Received October 7, 2009; Revised Manuscript Received January 24, 2010

ABSTRACT: A series of poly(meth)acrylamide derivatives with pendent six-member cyclic orthoester groups, i.e., poly(*N*-(2-alkyloxy-1,3-dioxan-5-yl)methacrylamide)s and poly(*N*-(2-alkyloxy-1,3-dioxan-5-yl)acrylamide)s, have been synthesized and characterized. The difference between these polymers lies in the type of alkyl substitutes (R^3), the stereochemical structures of the pendent cyclic orthoester groups (*trans* vs *cis*), and the main chain structures (polymethacrylamide vs polyacrylamide). Aqueous solution properties and pH-dependent hydrolysis behaviors of these polymers were studied by various methods including turbidimetry, fluorescence probe, DSC, ^{1}H NMR, microscopy, and light scattering. The results show that these polymers except P*t*NPM can be dissolved in water at low temperature, and all of the water-soluble polymers are thermosensitive with different lower critical solution temperatures (LCSTs) and susceptible to hydrolysis in mildly acidic conditions. Both thermosensitive properties and acid-triggered hydrolysis behaviors of the polymers are closely related to the polymer structures. In general, polymethacrylamides display higher cloud points (CPs) than polyacrylamides. In addition, the polymers with larger R^3 and *trans* configuration have a lower CP and greater magnitude of dehydration and exhibit a liquid−solid phase transition, while those with smaller R^3 and *cis* configuration have a smaller magnitude of dehydration and undergo a liquid−liquid phase separation. In addition, a two-stage transition process is observed for the polymers with R^3 being methyl. ^{1}H NMR results reveal that the acid-triggered hydrolysis rate of the pendent orthoesters increases as R^3 changed from methyl to isopropyl, and the configuration changed from *cis* to *trans*. The synergetic effect of R^3 and stereochemical structure of the pendent groups on the hydrolysis products of the polymers were also observed

Introduction

In recent years, stimuli-responsive polymers have attracted great interest worldwide due to their potential applications in various fields.[1] Among them, the thermoresponsive polymers, especially those with lower critical solution temperature (LCST), have been extensively investigated in both scientific and applied research areas because of the ease of controlling temperature.[2] Two types of most representative thermoresponsive polymers have been reported: the first one is poly(*N*-monoalkyl-substituted (meth)acrylamide)s and poly(*N*-vinylamide)s whose phase transitions are accompanied by the formation of inter- and/or intrachain hydrogen bond above their LCSTs;[3] the second one is poly(vinyl ether)s and poly(oligo(ethylene glycol) (meth)-acrylate)s which undergo a phase transition through thermally induced dehydration but without formation of the inter- and/or intrachain hydrogen bond in the polymer-rich phase.[4] Generally speaking, the LCST of a thermoresponsive polymer can be adjusted by tuning the hydrophilic/hydrophobic balance in the polymer. Changing the main chain structure, molecular weight, and chain end group of a homopolymer can regulate the LCST, but the easiest way is through copolymerization of different monomers.[5,6] However, a synergetic effect of various factors on the clouding points (CPs) is often observed; for example, the effect of α-methyl in the backbone on CP is also dependent on the pendent groups of poly(meth)acrylamide derivatives.[7]

*Corresponding author: e-mail zcli@pku.edu.cn; Tel 86-10-62755543; Fax 86-10-62751708.

pH/thermo doubly responsive polymers represent an important group of multiresponsive polymers due to their potential applications in biomedical and pharmaceutical areas. The most commonly used strategy to render a polymer with pH/thermo double responsivity is to incorporate reversibly ionizable groups in the polymer backbone or as the pendent groups by copolymerization or macromolecular reaction. Some monomers having ionizable groups and an appropriate amphiphilicity can also afford pH/thermo doubly responsive polymers.[2a] Recently, a novel type of thermoresponsive polymers that are susceptible to hydrolysis in acidic media was developed by introducing acid-labile linkages in the pendent groups[8] or the backbone.[9] We have reported the acid-labile thermoresponsive polymethacrylamides with pendent six-member cyclic orthoester groups whose LCSTs can be tuned by controlling the acid-triggered hydrolysis of the pendent groups.[8a] The acid-labile feature makes these polymers potentially applicable for constructing drug delivery systems that remain stable in blood but are capable of releasing their payload at the mildly acidic sites. Regarding the cyclic orthoester, 1,4-disubstitution makes the monomers have *trans* and *cis* isomers. In the previous paper, we reported the effect of stereochemical structure of the pendent moieties on the aqueous solution properties of thermoresponsive polymers.[8b] In the present work, a series of poly(meth)acrylamide derivatives with pendent six-member cyclic orthoester groups have been prepared (Scheme 1). These polymers are different in alkyl substitute (R^3) and stereochemical structure (*trans* vs *cis*) of the pendent groups as well as the main chain structure (R). It is found that these factors show a

 Published on Web 02/04/2010

Scheme 1. Synthesis of the Monomers and Polymers[a]

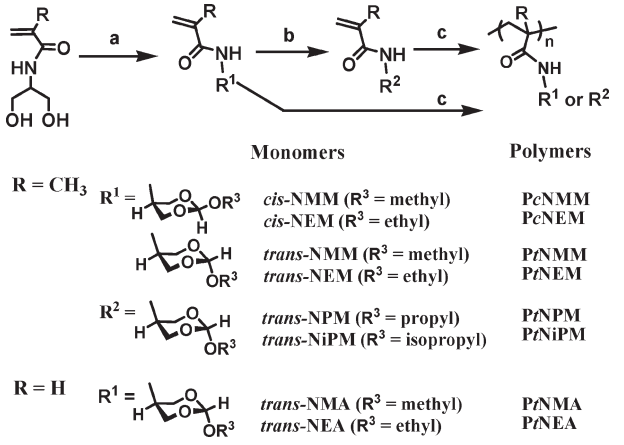

[a] Reagents and conditions: (a) trialkyl orthoformate, $TsOH \cdot H_2O$, rt; (b) (iso)propyl alcohol, toluene, 110 °C, ~12 h; (c) AIBN, 60 °C, 24 h in dioxane.

synergetic effect on the aqueous solution properties of the polymers, including thermally induced phase transition and acid-triggered hydrolysis behaviors.

Experimental Section

Materials. 2-Amino-1,3-propanediol (Huaqingrunde Co., Beijing, China), triethyl orthoformate, trimethyl orthoformate, D_3PO_4, D_3CO_2D, NaOD, and D_2O (Acros) were used as received. 1,4-Dioxane and tetrahydrofuran (THF) were distilled over sodium prior to use. 2,2′-Azobis(isobutyronitrile) (AIBN) was recrystallized twice from methanol. $CDCl_3$ (Acros) was treated with anhydrous Na_2CO_3 before NMR measurements for the orthoester-containing samples. Pyrene (Py, Acros) was recrystallized from ethanol twice. (Meth)acryloyl chloride was synthesized from (meth)acrylic acid and benzoyl chloride according to the literature.[10] *N*-(1,3-Dihydroxypropan-2-yl)methacrylamide and *N*-(1,3-dihydroxypropan-2-yl)acrylamide were synthesized by a similar procedure as reported previously.[6a] Other solvents and reagents were purchased from Beijing Chemical Reagent Co. and used as received.

Synthesis of Monomers. *trans*-NEM, *cis*-NEM, and *trans*-NEA were prepared by the same procedure as reported previously.[8b,11] *trans*-NMM, *cis*-NMM, and *trans*-NMA were prepared by the similar procedure as for their analogues with R^3 being ethyl, using trimethyl orthoformate instead of triethyl orthoformate in the first step (Scheme 1). *trans*-NiPM and *trans*-NPM were prepared from NMM (a mixture of *trans* and *cis* isomers) by replacing the methoxy group with isopropoxy and propoxy groups, respectively. Take the synthesis of *trans*-NiPM as an example, the procedure is as follows: Briefly, 4.5 g (75 mmol) of isopropyl alcohol and 50 mg of 4-methoxyphenol were added to a 500 mL flask containing 3.0 g (15 mmol) of NMM, 37 mg (0.15 mmol) of pyridinium *p*-toluenesulfonate, and 200 mL of toluene. After the mixture was refluxed under magnetic stirring for 6 h, most of the toluene was removed by rotary evaporation. The residue was prepurified through an Al_2O_3 column using a mixture of ethyl acetate and petroleum ether (1/5, v/v) to afford 0.7 g of crude product. Recrystallization from a mixed solvent of THF and hexane produced a white powder (0.66 g, 19% yield). *trans*-NPM was prepared by a similar procedure with a yield of 20%.

trans-NMM. ^{1}H NMR (TMS, $CDCl_3$, 400 MHz, ppm, Figure S1A): 6.72 (s, 1H, −N*H*CO−), 5.77 (s, 1H, *H*−CH=C(CH_3)−), 5.39 (s, 1H, *H*−CH=C(CH_3)−), 5.35 (s, 1H, C*H*O_3), 4.37 (d, 2H, J = 11.6 Hz, −NHCH(CH_2)$_2$, axial), 4.0 (m, 1H, −NHC*H*-(CH_2)$_2$), 3.64 (d, 2H, J = 11.6 Hz, −NHCH(CH_2)$_2$, equatorial), 3.38 (s, 3H, −OCH_3), 2.00 (s, 3H, CH_2=C(CH_3)−). ^{13}C NMR ($CDCl_3$, 75 MHz, ppm, Figure S1B): 168.0 (−*C*=O), 139.8 (CH_2=*C*(CH_3)−), 120.0 (*C*H_2=C(CH_3)−), 108.3 (−*C*HO_3), 61.9 (−NHCH(*C*H_2)$_2$), 53.0 (−O*C*H_3), 43.5 (−NH*C*H-(CH_2)$_2$), 18.5 (CH_2=C(*C*H_3)−). FT-IR (KBr, cm^{-1}): 3306, 3053, 2974, 2929, 2885, 1657, 1622, 1537, 1380, 1212, 1152, 1077, 1051, 1016. MS (m/z): 200 (M − 1)$^+$. mp 80.7−82.4 °C.

cis-NMM. ^{1}H NMR (TMS, $CDCl_3$, 400 MHz, ppm, Figure S2A): 6.58 (s, 1H, −N*H*CO−), 5.75 (s, 1H, *H*−CH=C(CH_3)−), 5.38 (s, 1H, *H*−CH=C(CH_3)−), 5.20 (s, 1H, C*H*O_3), 4.02 (s, 4H, −NHCH(CH_2)$_2$), 4.00 (m, 1H, −NHC*H*(CH_2)$_2$), 3.60 (s, 3H, −OCH_3), 1.99 (s, 3H, CH_2=C(CH_3)−). ^{13}C NMR ($CDCl_3$, 75 MHz, ppm, Figure S2B): 168.0 (−*C*=O), 139.8 (CH_2=*C*-(CH_3)−), 120.2 (*C*H_2=C(CH_3)−), 112.1 (−*C*HO_3), 68.1 (−NH-CH(*C*H_2)$_2$), 53.3 (−O*C*H_3), 42.8 (−NH*C*H(CH_2)$_2$), 18.5 (CH_2=C(*C*H_3)−). FT-IR (KBr, cm^{-1}): 3299, 2955, 2890, 1655, 1619, 1556, 1212, 1141, 1074, 1039, 973. MS (m/z): 200(M − 1)$^+$. Elemental analysis ($C_9H_{15}NO_4$): Calcd: C % 53.72, N % 6.96, H % 7.51. Found: C % 53.54, N % 6.86, H % 7.59. mp 98.6−99.8 °C.

trans-NiPM. ^{1}H NMR (TMS, $CDCl_3$, ppm, Figure S3A): 6.74 (s, 1H, −N*H*CO−), 5.77 (s, 1H, *H*−CH=C(CH_3)−), 5.53(s, 1H, C*H*O_3), 5.39 (s, 1H, *H*−CH=C(CH_3)−), 4.39 (d, 2H, J = 11.5 Hz, −NHCH(CH_2)$_2$, axial), 4.00 (m, 1H, −NHC*H*(CH_2)$_2$), 3.90 (m, 1H, −OCH*H*(CH_3)$_2$), 3.64 (d, 2H, J = 11.5 Hz, −NHCH(CH_2)$_2$, equatorial), 2.00 (s, 3H, CH_2=C-(CH_3)−), 1.24 (d, 6H, J = 5.21 Hz, −OCHH(CH_3)$_2$). ^{13}C NMR ($CDCl_3$, 75 MHz, ppm, Figure S3B): 167.9 (−*C*=O), 139.7 (CH_2=*C*(CH_3)−), 120.1 (*C*H_2=C(CH_3)−), 106.2 (−*C*HO_3), 67.4 (−O*C*H(CH_3)$_2$), 62.0 (−NHCH(*C*H_2)$_2$), 43.6 (−NH*C*H-(CH_2)$_2$), 22.2 (−OCH(*C*H_3)$_2$), 18.5 (CH_2=C(*C*H_3)−). FT-IR (KBr, cm^{-1}): 3283, 2976, 2875, 1652, 1617, 1541, 1391, 1227, 1151, 1108, 978. MS(m/z): 228 (M − 1)$^+$. Elemental analysis ($C_{11}H_{19}NO_4$): Calcd: C % 57.62, N % 6.11, H % 8.35. Found: C % 57.31, N % 6.00, H % 8.15. mp 69.5−72.3 °C.

trans-NPM. ^{1}H NMR (TMS, $CDCl_3$, 400 MHz, ppm, Figure S4A): 6.73 (s, 1H, −N*H*CO−), 5.78 (s, 1H, *H*−CH=C(CH_3)−), 5.44 (s, 1H, C*H*O_3), 5.39 (s, 1H, *H*−CH=C(CH_3)−), 4.39 (d, 2H, J = 11.3 Hz, −NHCH(CH_2)$_2$, axial), 4.01 (m, 1H, −NHC*H*(CH_2)$_2$), 3.64 (d, 2H, J = 11.3 Hz, −NHCH(CH_2)$_2$, equatorial), 3.49 (t, 2H, J = 6.80 Hz, −OCH_2CH_2CH_3), 2.00 (s, 3H, CH_2=C(CH_3)−), 1.67 (m, 2H, −OCH_2CH_2CH_3), 0.98 (t, 2H, J = 7.28 Hz, −OCHH_2CH_2CH_3). ^{13}C NMR ($CDCl_3$, 75 MHz, ppm, Figure S4B): 168.0 (−*C*=O), 139.8 (CH_2=*C*(CH_3)−), 120.0 (*C*H_2=C(CH_3)−), 107.5 (−*C*HO_3), 67.4 (−O*C*H_2CH_2CH_3), 62.0 (−NHCH(*C*H_2)$_2$), 43.6 (−NH*C*H-(CH_2)$_2$), 22.5 (−OCH_2*C*H_2CH_3), 18.5 (CH_2=C(*C*H_3)−), 10.6 (−OCH_2CH_2*C*H_3). FT-IR (KBr, cm^{-1}): 3285, 2978, 2927, 2875, 1655, 1621, 1545, 1162, 1037, 976, 917. MS (m/z): 228 (M − 1)$^+$. Elemental analysis ($C_{11}H_{19}NO_4$): Calcd: C % 57.62, N % 6.11, H % 8.35. Found: C % 57.49; N% 6.08, H% 8.70.

trans-NMA. ^{1}H NMR (TMS, $CDCl_3$, 400 MHz, ppm, Figure S5A): 6.54 (s, 1H, −N*H*CO−), 6.33 (d, 1H, J = 17.6 Hz, *H*−CH=CH−), 6.18 (m, 1H, CH_2=C*H*−), 5.70 (d, 1H, J = 9.9 Hz, *H*−CH=CH−), 5.35 (s, 1H, C*H*O_3), 4.38 (d, 2H, J = 11.3 Hz, −NHCH(CH_2)$_2$, axial), 4.04 (m, 1H, −NHC*H*(CH_2)$_2$), 3.63 (d, 2H, J = 11.3 Hz, −NHCH(CH_2)$_2$, equatorial), 3.38 (s, 3H, −OCH_3). ^{13}C NMR ($CDCl_3$, 75 MHz, ppm, Figure S5B): 165.0 (−*C*=O), 130.6 (CH_2=*C*H−), 127.1 (*C*H_2=CH−), 109.3 (−*C*HO_3), 62.0 (−NHCH(*C*H_2)$_2$), 53.1 (−O*C*H_3), 43.5 (−NH*C*H(CH_2)$_2$). FT-IR (KBr, cm^{-1}): 3252, 3065, 2932, 1654, 1619, 1553, 1141, 1086, 1036. MS (m/z): 186 (M − 1)$^+$. Elemental analysis ($C_8H_{13}NO_4$): Calcd: C % 51.33, N % 7.48, H % 7.00. Found: C % 51.42, N % 7.30, H % 7.07. mp 101.5−103.0 °C.

Polymerization. All of the monomers were polymerized using AIBN as the initiator. Briefly, monomer, AIBN (1.0 mol % relative to the monomer), and dried dioxane were added sequentially to a polymerization tube. After dissolution of the monomer (~0.1 g/mL) by shaking, three cycles of freeze−pump−thaw were applied to remove oxygen, and the tube was

Table 1. Characterizations of the Orthoester-Containing Poly(meth)acrylamides and Their Aqueous Solution Properties

	yield (%)	M_w[a] ($\times 10^4$)	PDI[a]	CP[b] (°C)	T_{max}[c] (°C)	ΔH[d] (kJ/mol)	CAC[e] (mg/mL)
P*t*NMM	68	3.8	1.6	40.6			n.d.
P*c*NMM	67	2.5	2.0	55.1			n.d.
P*t*NEM[f]	91	5.5	1.7	18.8	17.6	6.1	0.10
P*c*NEM[f]	56	5.2	1.8	21.9	20.8	1.3	0.40
P*t*NiPM	90	4.9	1.5	11.5	9.8	6.0	0.06
P*t*NPM	60	4.3	1.8				
P*t*NMA	65	4.7	2.0	36.3			n.d.
P*t*NEA	70	5.5	1.8	12.0	9.7	5.0	n.d.

[a] Determined by GPC with THF as an eluent and monodisperse polystyrenes as the standards. [b] Defined as the inflection point of the transmittance vs temperature plot in pH 8.4 PB, heating rate: 1.0 °C/min, polymer concentration: 1.0 mg/mL. [c] Defined as the maximum of the endothermic peak, 4.0 wt % in pH 8.4 PB, heating rate: 1.0 °C/min. [d] Calorimetric enthalpy in kJ/mol per repeating units (heating process). [e] Measured by fluorescence method (Figure S12, I_{338}/I_{333} vs concentration plots). n.d. means not detected. [f] For P*t*NEM and P*c*NEM, the data (except CAC) have been reported in a previous paper (ref 8b).

sealed in vacuo. The polymerization was carried out at 60 °C for 24 h. The polymers were recovered by twice precipitation from diethyl ether, dried in vacuo, and characterized using gel permeation chromatography (GPC) and ^{1}H NMR.

Measurements. GPC measurements were carried out on an equipment with a Waters 1525 binary HPLC pump, a Waters 2414 refractive index detector, and three Waters Styragel columns (HT2, HT3, and HT4). THF was used as the eluent at a flow rate of 1.0 mL/min (35 °C). A series of narrow dispersed polystyrenes were used as the standards. A Bruker 400 MHz spectrometer was used to record ^{1}H NMR spectra of the monomers and polymers in $CDCl_3$ (TMS as the internal reference). ^{13}C NMR spectra in $CDCl_3$ and ^{1}H NMR spectra in the deuterated buffers were recorded on a Varian Mercury Plus 300 MHz NMR spectrometer. Differential scanning calorimetry (DSC) measurements were performed on TA Instruments DSC Q100. 10 μL of the polymer solution (4.0 wt %, 10 mM phosphate buffer (PB)) was sealed in an aluminum pan in order to minimize water evaporation. An aluminum pan with free buffer (10 μL) was used as the reference. Scanning rate was 1.0 °C/min. The phase transition temperature (T_{max}) was defined as the maximum of the endothermic peak. The transition enthalpy (ΔH) was measured from the endothermic peak area using an indium standard. The transmittance of polymer solution (10 mM PB, pH 8.4) was detected at 500 nm in a 1 cm square quartz cell on a Shimadzu 2101 UV−vis spectrometer equipped with a water-jacketed cell holder and a circulating water bath (Shimadzu TB-85). Polymer-free 10 mM PB was used as a reference. Cloud point (CP) was defined as the inflection point of the transmittance vs temperature curve which was determined by the maximum in the first derivative. Fluorescence measurements were carried out on a Hitachi F-4500 fluorescence spectrometer. For emission spectra, the excitation and emission slit widths were 5.0 and 2.5 nm, respectively, with an excitation wavelength of 339 nm. For excitation spectra, both excitation and emission slit widths were set at 5.0 nm, with an emission wavelength of 390 nm. Scanning rate was 240 nm/min. The polymer solutions with Py (5.0×10^{-7} mol/L) were prepared as reported previously.[8b] I_1/I_3 was defined as the intensity ratio of the first (~375 nm) to the third (~385 nm) bands in the emission spectrum. Because the polymer solutions were turbid at high concentrations, light scattering of the aggregate particles had a strong effect on the emission spectra. In order to reduce the magnitude of this influence, the intensities of the first and the third bands were subtracted by the intensity at 362 nm for calculating I_1/I_3. Microscopic observations of the polymer aqueous solutions were carried out using a Leica DLMP microscope. Laser light scattering experiments were carried out using a commercial spectrometer (Brookhaven Inc., Holtsville, NY) equipped with a BI-200SM goniometer and a BI-TurboCorr digital correlator. A 200 mW vertically polarized solid-state laser (532 nm, CNI, Changchun, China) was used as the light source. In dynamic light scattering, the intensity−intensity time autocorrelation function was measured in the self-beating mode. The Laplace inversion program, CONTIN, was applied to obtain the average line width Γ and its distribution at varying scattering angle q. The apparent hydrodynamic radius ($R_{h,app}$) was obtained by extrapolating Γ/q^2 to zero angle, followed by the calculation based on Stokes−Einstein equation.[11] In the present work, pH 8.4 PB was used in order to avoid or reduce hydrolysis of the orthoester groups during the measurements, except for the pH-dependent hydrolysis experiments.

pH-Dependent Hydrolysis. For hydrolysis monitored by the turbidimetric method, each of the polymers was dissolved in cold 10 mM pH 8.4 PB (1.0 mg/mL). After being maintained at 37 °C for ~10 min, the transmittance of the solution was decreased to 0%, using the polymer-free PB as a reference (100% transmittance). Then, the polymer solution was adjusted to pH 4.0 by adding 5.0 M pH 4.0 acetate buffer (0 time point), and the transmittance was measured against time at 37 °C. For hydrolyses at other pH, different concentrated acetate buffers with various pH (4.6, 5.0, 5.4) were used. For hydrolysis (pD 5.0) monitored by NMR spectrometry, the polymer solution at pD 8.4 was first maintained at 37 °C for 15 min, and the measured ^{1}H NMR spectrum was used as that of the 0 time point. After adding 5.0 M acetate buffer (pD 5.0), the polymer solution was quickly mixed and maintained at 37 °C. The ^{1}H NMR spectra were recorded at specific time points.

Results and Discussion

The polymethacrylamide derivatives with pendent six-member cyclic orthoester groups are a new type of thermo/pH doubly responsive polymers. We have already reported the effect of stereochemical structures of the pendent groups on their solution properties. To systematically investigate the effects of other parameters, we designed and synthesized a series of polymers. These polymers are different in side chain alkyl substitutes (P*t*NMM, P*t*NEM, P*t*NiPM, and P*t*NPM), stereochemical structures (P*t*NMM vs P*c*NMM, P*t*NEM vs P*c*NEM), and polymer main chain (P*t*NMM vs P*t*NMA, P*t*NEM vs P*t*NEA). Syntheses of monomers *trans*-NEM and *cis*-NEM were reported previously.[8b] *trans*-NMM and *cis*-NMM were synthesized by the similar procedure using trimethyl orthoformate instead of triethyl orthoformate. Monomers *trans*-NPM and *trans*-NiPM were prepared from NMM by replacing the methoxy group with propoxy and isopropoxy groups, respectively. Acrylamide monomers (*trans*-NMA and *trans*-NEA) were prepared by the similar procedure as for their mathacrylamide analogues (Scheme 1).[11] All polymers were prepared by conventional free radical polymerization of the monomers (Table 1, Figures S6−S11).

Aggregation of the Polymers below LCST. All the polymers except P*t*NPM are water-soluble at low temperature (5 °C) but show obvious LCST upon increasing temperature. We have reported previously that even at a temperature below their individual LCST, the transmittance of P*t*NEM and P*c*NEM solutions decreased with increasing the polymer

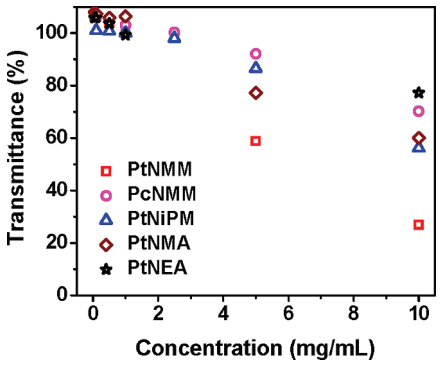

Figure 1. Transmittance of P*t*NMM, P*c*NMM, P*t*NiPM, P*t*NMA, and P*t*NEA aqueous solutions in 10 mM pH 8.4 PB at various concentrations. λ = 500 nm; 5 °C.

concentration, which was attributed to the presence of colloidal aggregates.[8b] We measured the concentration-dependent transmittance change of all the other water-soluble orthoester-containing poly(meth)acrylamides at 5 °C, and the results are summarized in Figure 1. Visually transparent solutions (>90 T%) can be obtained when the polymer concentration was 2.5 mg/mL or below. At higher concentrations, for example 10 mg/mL, the solution became translucent or opaque, depending on the polymers. In fact, bimodal size distributions were clearly observed for P*t*NMM, P*c*NMM, and P*t*NEA even at a much lower concentration of 0.1 mg/mL by dynamic light scattering (DLS) measurements (data not shown). These results demonstrate that the presence of some colloidal loose aggregates below their LCST is a common feature for these poly(meth)-acrylamides.

The aggregation of P*t*NiPM below its LCST was further investigated using pyrene (Py) as a fluorescence probe. Py is a well-known fluorescent probe whose fluorescence emission and excitation spectra are very sensitive to the microenvironment.[12] For the emission spectrum of Py, it is commonly considered that the intensity ratio of the first to the third bands (I_1/I_3) decreases as the polarity of its local environment is reduced.[12a] In the excitation spectrum of Py, the (0,0) band at ca. 334 nm shifts to a longer wavelength when Py molecules are transferred into a less polar and/or a confined microenvironment.[12b] Thus, the emission and excitation spectra of Py are widely used to study the aggregation behaviors of amphiphilic (co)polymers in water, including the measurement of critical aggregation concentration (CAC).[6c,13] Figure 2 shows the normalized emission and excitation spectra of Py in P*t*NiPM aqueous solutions with various polymer concentrations at 5 °C. It can be seen that I_1/I_3 decreased, and the (0,0) band red-shifted ca. 2.5 nm with the increase of polymer concentration, indicating that Py molecules were partitioned into a relatively hydrophobic microenvironment.[8b] From the plots of I_{338}/I_{333} vs polymer concentration, CAC of P*t*NiPM was obtained to be ca. 0.06 mg/mL, which is smaller than that of P*t*NEM (0.10 mg/mL, Figure S12 and Table 1). This means that P*t*NiPM has a stronger aggregation tendency than P*t*NEM, which is reasonable considering the more hydrophobic nature of isopropyl group compared to ethyl group. As shown in Figure 2A, a broad featureless excimer emission peak centered at ca. 475 nm was also observed. The intensity ratio of the excimer to monomer emission was dependent on the polymer concentration, which can be attributed to the distribution of Py molecules between the associated microdomains formed by P*t*NiPM and the bulk water phase.[8b]

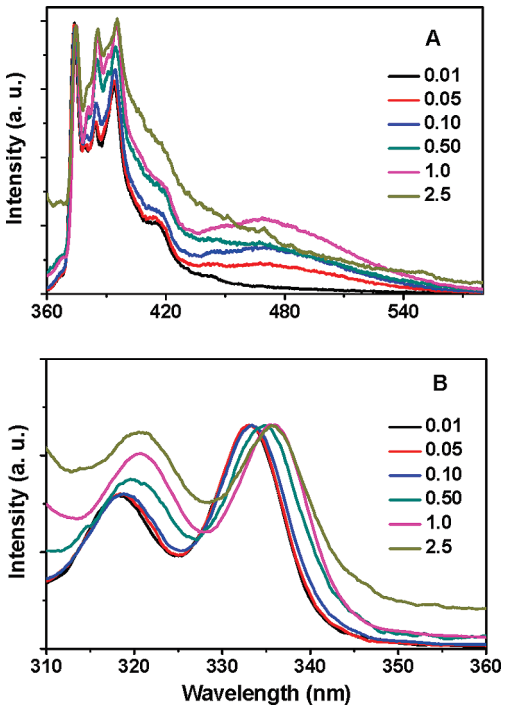

Figure 2. Normalized emission (A) and excitation (B) spectra of Py in P*t*NiPM aqueous solution (10 mM pH 8.4 PB) at various polymer concentrations (mg/mL). λ_{ex} = 339 nm; 5 °C; Py concentration: 5.0×10^{-7} mol/L.

Thermally Induced Phase Transition. Phase transition behaviors of the polymer aqueous solutions were first investigated by the turbidimetric method. Shown in Figure 3 are the transmittance vs temperature plots of the polymer solutions (1.0 mg/mL) in a heating/cooling cycle. It is seen that all the polymers, except P*c*NMM and P*t*NMA, showed a highly sensitive and reversible phase transition at a specific temperature. For the polymethacrylamides with *trans* configuration, the CP decreased from 40.6 °C for P*t*NMM to 18.8 °C for P*t*NEM, and to 11.5 °C for P*t*NiPM. Upon cooling, obvious hysteresis was observed for P*t*NiPM while P*t*NMM hardly displayed hysteresis (Figure 3A). This phenomenon can again be ascribed to the more hydrophobic nature of isopropyl group than that of methyl or ethyl group (Scheme 1). Above its phase transition temperature, P*t*NiPM chains may adopt a more compact conformation in the aggregates due to the stronger hydrophobic interaction of the isopropyl groups. As a result, the intra- and interchain hydrogen bonding between the amide groups as well as the chain entanglement in the polymer aggregates were enhanced, which was proposed to be the reason for hysteresis.[14] In a recent report it was clearly demonstrated that the local environment of poly(*N*-isopropylacrylamide) (PNIPAM) chains drastically affected the formation of hydrogen bonds between the amide groups.[15] By comparing the other two pairs of polymers, P*c*NMM vs P*c*NEM and P*t*NMA vs P*t*NEA, we can see that the CP also increased when changing R^3 from ethyl to methyl (Figure 3B,C). Regarding the effect of stereochemical structure on the CP, like PNEM polymers,[8b] P*c*NMM showed a higher CP than P*t*NMM. The CP difference between P*c*NMM and P*t*NMM was more significant than that between P*c*NEM and P*t*NEM. (Figure 3A,B and Table 1). Comparison of the CPs of P*t*NMM with P*t*NMA or P*t*NEM with P*t*NEA indicated that the phase transition of the polyacrylamides occurred at a lower temperature than that of the corresponding

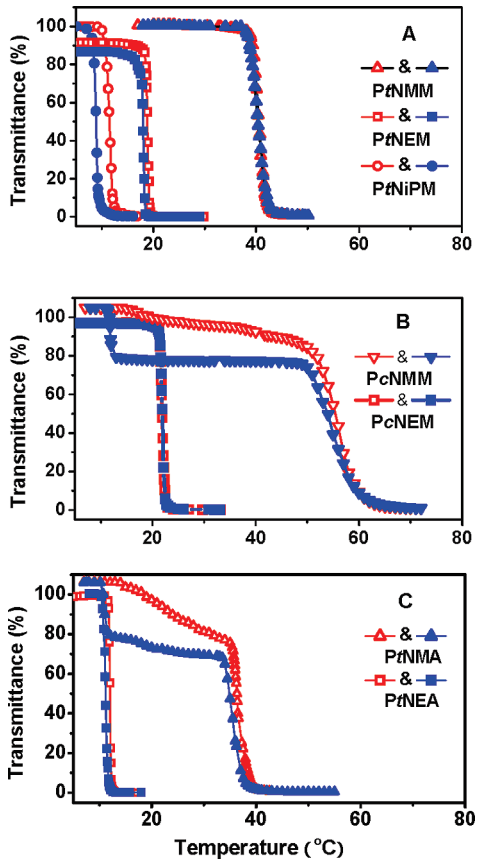

Figure 3. Transmittance vs temperature plots of the polymethacrylamides with *trans* (A) and *cis* (B) structures and the polyacrylamides with *trans* structures (C) in 10 mM pH 8.4 PB (1.0 mg/mL) in a heating (empty) and cooling (solid) process. λ = 500 nm; heating/cooling rate: ca. 1.0 °C/min. The plots for P*t*NEM and P*c*NEM have been used in a previous paper (ref 8b).

polymethacrylamides (Table 1). Similar results were also obtained for other thermoresponsive polymers.[7,16] This irregular phenomenon could be attributed to the steric hindrance of the methyl groups in the polymer backbone which restrict the intrachain collapse and interchain association.[7a,b]

The effect of polymer concentration on the phase transition/separation behaviors was also studied (Figure 4 and Figure S13). For P*t*NMM, P*c*NMM, and P*t*NMA, their CPs initially decreased significantly with increasing the polymer concentration and then became constant at the higher concentration range. In the case of P*t*NiPM and P*t*NEA, the same trend was obtained but with a much smaller magnitude of CP variation. A similar phenomenon was reported for P*t*NEM and P*c*NEM as well as for other thermosensitive polymers, which can be ascribed to the fact that the high polymer concentrations would macroscopically favor the flocculation of the primary aggregates.[8b,17]

The thermally induced phase transition behaviors of these polymers were further studied by DSC and ^{1}H NMR. Shown in Figure 5 are DSC thermograms of the polymer aqueous solutions at a 4.0 wt % concentration in the heating process. It is seen that all three polymers with R^3 being the methyl group did not show detectable endothermic peak at CP, indicating that these polymers have a small magnitude of dehydration during their phase separation. Each of the other four polymers showed an obvious endothermic peak with the phase transition temperature (T_{max}) being 1−2 °C lower than their respective CP. The phase transition enthalpies (ΔHs) of these polymers were calculated from the peak areas

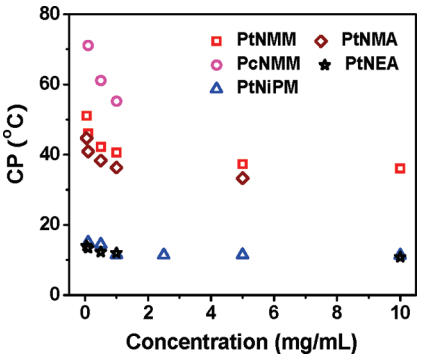

Figure 4. Concentration dependence of the CPs of P*t*NMM, P*c*NMM, P*t*NiPM, P*t*NMA, and P*t*NEA.

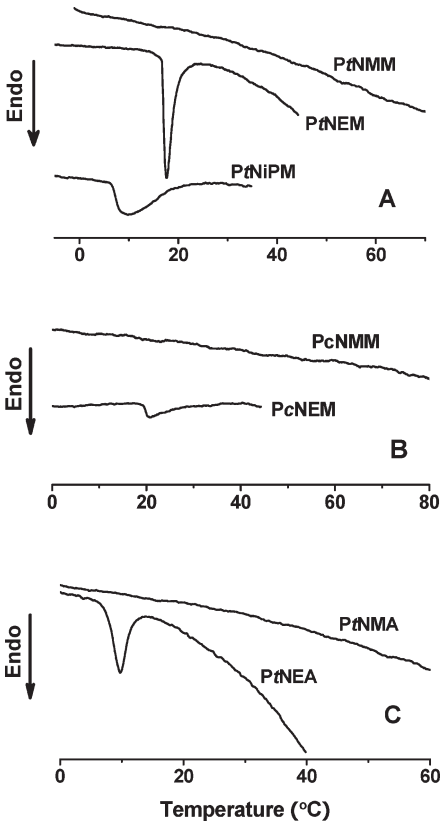

Figure 5. DSC thermograms of the polymers in 10 mM pH 8.4 PB (40 mg/mL) with a heating rate of 1.0 °C/min. The DSC data for P*t*NEM and P*c*NEM have been presented in a previous paper (ref 8b).

(Table 1). Although the ΔHs of P*t*NEM and P*t*NiPM were almost the same, indicating that they had a similar magnitude of dehydration, their dehydration behaviors were quite different. The endothermic peak of P*t*NEM was very sharp with a maximum half-width of 1.9 °C, while P*t*NiPM had a much broad peak with a maximum half-width of 7.5 °C. This might be due to the stronger steric hindrance of isopropyl group compared to the relatively smaller ethyl group, which would reduce the cooperativity of P*t*NiPM chains in the phase transition. From Table 1 and Figure 5 it can also be seen that the ΔHs of P*t*NEM, P*t*NiPM, and P*t*NEA are comparable to that of PNIPAM (5−8 kJ/mol), which has a typical coil−globule phase transition.[3a] However, although an endothermic peak was detectable for P*c*NEM, its ΔH (1.3 kJ/mol) was very small, demonstrating an incomplete dehydration of the polymer chains even above the CP.[8b]

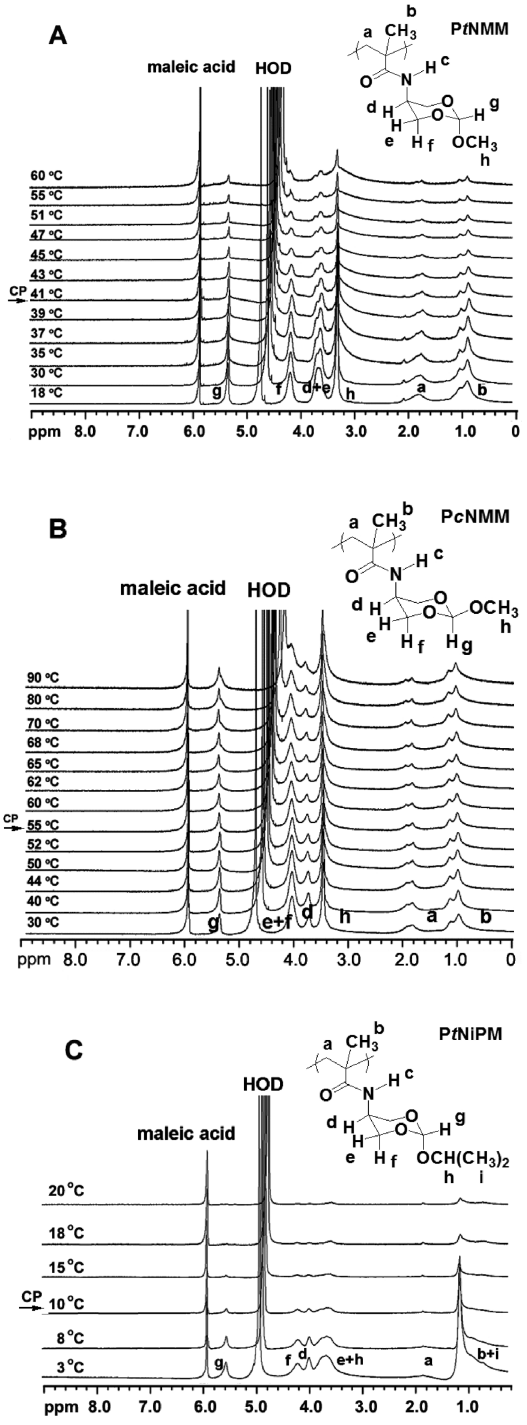

Figure 6. Temperature-dependent ^{1}H NMR spectra of P*t*NMM (A), P*c*NMM (B), and P*t*NiPM (C) in deuterated PB (10 mM, pD 8.4). The spectra were normalized at the proton signal (~6 ppm) of maleic acid, which was used as the internal standard.

Figure 6 shows the ^{1}H NMR spectra of P*t*NMM, P*c*NMM, and P*t*NiPM in D_2O at different temperatures. Below their CPs all the three polymers were well solvated, and the proton signals of the pendent groups and backbone were clearly observed. For P*t*NiPM, the signal intensities abruptly decreased around its CP with increasing the temperature. At 20 °C, a temperature of 9 °C above its CP, the peaks almost disappeared. By contrast, although the signal intensities of P*t*NMM were obviously reduced around its CP, the peaks could be clearly detectable even at 60 °C, a temperature of 20 °C above its CP. In the case of P*c*NMM,

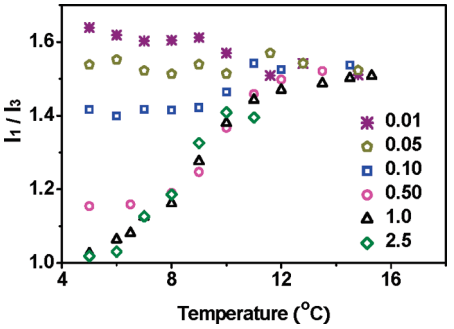

Figure 7. Temperature-dependent changes in I_1/I_3 of Py in P*t*NiPM solution (10 mM pH 8.4 PB) at various polymer concentrations (mg/mL).

there was no observable change in the ^{1}H NMR spectra around its CP (55.1 °C). Upon increasing temperature from 30 to 90 °C, the signal peaks were a little broadened but with no obvious decrease in the signal intensities (Figure 6B). On the basis of DSC and ^{1}H NMR measurements, it can be deduced that the polymers with pendent methyl group (R^3) underwent a liquid−liquid phase separation followed by the formation of coacervate droplets while the polymers with large ΔH; i.e., P*t*NEM, P*t*NiPM, and P*t*NEA likely showed a liquid−solid phase transition in the heating process. This speculation was further evidenced by the microscopic observations of the polymer solutions (Figure S14). Above the CPs, coacervate droplets can be seen in the aqueous solutions of P*t*NMM, P*c*NMM, and P*t*NMA while solidlike precipitates were formed for P*t*NEM, P*t*NiPM, and P*t*NEA. In the case of P*c*NEM, although an endothermic peak was detected, this polymer exhibited a liquid−liquid phase separation due to its small ΔH.[8b]

Py as a fluorescent probe was also applied to study the thermoresponsive behaviors of P*t*NiPM aqueous solution. Figure 7 shows I_1/I_3 of Py in P*t*NiPM solution as a function of temperature. The change of I_1/I_3 with temperature strongly depends on the polymer concentration. Below the CAC, I_1/I_3 showed an abrupt drop around its LCST (ca. 10 °C) upon heating, meaning the transfer of Py molecules into the collapsed polymer-rich phase. By contrast, at concentrations above the CAC, I_1/I_3 sharply increased when the temperature was raised through the LCST, indicating that the environmental polarity sensed by Py increased. A similar phenomenon was also found for the hydrophobically modified PNIPAM derivatives[18] as well as for P*t*NEM and P*c*NEM.[8b] As aforementioned, below its LCST, P*t*NiPM formed some kind of aggregates (above CAC) which can solvate Py molecules. When the temperature was raised through the LCST, dehydration of P*t*NiPM chains may induce the change in morphology of the original aggregates, resulting in the newly formed polymer-rich aggregates that can still accommodate Py molecules but are more polar in nature.

When we take a closer look at the transmittance curves as a function of temperature (Figure 3B,C), an interesting phenomenon was observed. A two-stage transition process occurred for the aqueous solutions of P*c*NMM and P*t*NMA, the two polymers with R^3 being methyl. Upon heating, the transmittance of the clear solution of P*c*NMM started to drop at ca. 15 °C (T_1, the first transition temperature) and decreased gradually to ca. 82% at 51 °C (T_2, the second transition temperature, approximately equal to the CP of P*c*NMM as shown in Table 1), beyond which a sharp decrease in transmittance occurred. The two-stage process became more obvious in the cooling process. The turbid

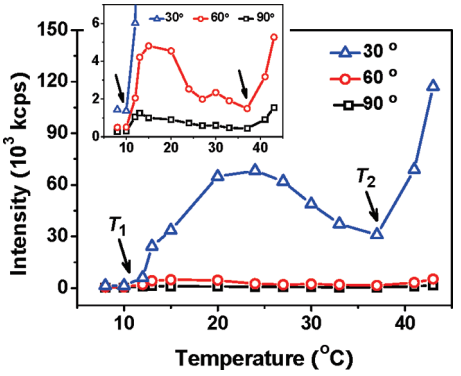

Figure 8. Temperature dependence of the scattered light intensity of P*t*NMA in 10 mM pH 8.4 PB (0.5 mg/mL) at various detection angles.

solution became bluish as the temperature decreased to T_2 with only a little hysteresis. Upon further cooling from T_2, a strong hysteresis was observed. The transmittance (ca. 76%) remained unchanged until 12.4 °C, a temperature close to T_1 where the solution suddenly became clear. In the case of P*t*NMA, similar results were obtained. The ratio of the two transitions depends on the polymer concentration: the higher the concentration, the more obvious the first transition (Figures S13D and S15). The two-stage transition process can also be observed for P*t*NMM when the concentration was increased to 10 mg/mL (Figure S13A).

Laser light scattering measurements were performed to further investigate this unique phenomenon. Figure 8 shows the temperature dependence of the excess scattered intensity of P*t*NMA at 0.5 mg/mL. The solution was equilibrated at each temperature for ca. 30 min before measurements. Clearly, two transitions, indicated as T_1 (ca. 11 °C) and T_2 (ca. 37 °C) in Figure 8, were observed regardless of the detection angle. A sharp increase in the excess scattered intensity occurred at temperature above T_2, where significant increase in turbidity was observed above 40 °C (Figure 3C). CONTIN analysis also revealed existence of two particle populations in P*t*NMA solution at temperatures below T_2 (Figure 9A). The smaller components, $R_{h,app}$ of which remained almost constant at about 5 nm, were attributed to individual P*t*NMA chains. The larger components, whose size increased with temperature, were assigned to the polymer associates formed by P*t*NMA chains. The disappearance of single polymer chains at a temperature above T_2 also suggested that the second transition was more pronounced than the first one. Figure 9B shows the evolutional increase in the size of the associate or aggregate as a function of temperature. Two increases in $R_{h,app}$ were clearly observed at T_1 and T_2, confirming the two-stage transition process. We have also studied the thermally induced phase transition behaviors of P*t*NEM, P*c*NEM, and P*t*NEA by using light scattering. Only one-stage transition was observed around their individual CPs (Figures S16). Regarding the double or multistage transitions of thermoresponsive polymers, there are some reports in the literature.[19] However, most of papers focus on the diblock copolymers composed of one LCST block and one UCST (upper critical solution temperature) block at different critical temperatures[19a−d] or the block copolymers composed of various thermoresponsive blocks that show different LCSTs.[19e−i] In addition, double phase transitions were observed when PNIPAM was densely grafted onto the surface of gold nanoparticles[19j] or the periphery of a hyperbranched polyester core.[19k] The two transitions at lower and higher temperatures were attributed to the collapse of the inner and outer region of the PNIPAM corona,

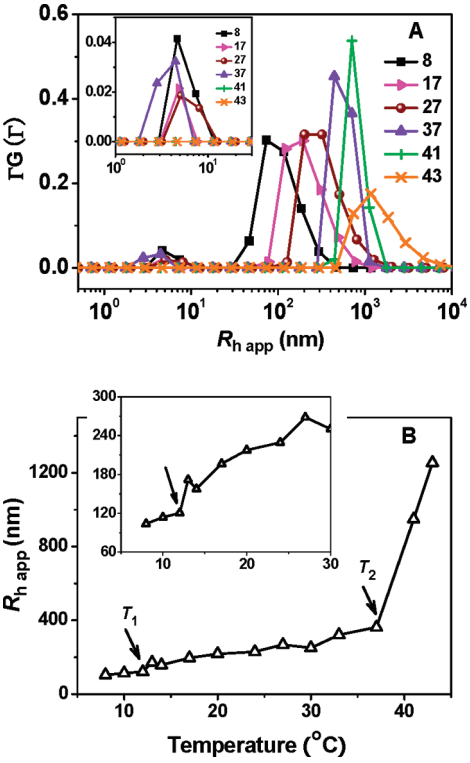

Figure 9. (A) CONTIN analysis of P*t*NMA in 10 mM pH 8.4 PB (0.5 mg/mL) at different temperatures at 30°. (B) Temperature dependence of $R_{h,app}$ of the polymer associates in P*t*NMA aqueous solution.

respectively.[19k] In our case, the two-stage transitions were observed only for the homopolymers with R^3 being methyl but not for those with R^3 being ethyl or isopropyl, regardless of the *trans*/*cis* configuration or the main-chain structure. A clear and conclusive explanation of this unique phenomenon is now still premature. We speculate that the two transitions are caused by the differentiated and sequential dehydration of the orthoester and amide groups. For the polymers with R^3 being ethyl or isopropyl, the orthoester groups are more hydrophobic and less hydrated, and therefore only dehydration of the amide groups could be detected, resulting in one-stage transition. In the case of R^3 being methyl, however, the orthoester groups are more hydrophilic, and their hydration is enhanced; a transition caused by dehydration of these groups is detectable at T_1. Pronounced chain collapse and aggregation were not achieved until the temperature increased to T_2, at which the dehydration of the amide groups occurred.

pH-Dependent Hydrolysis. The water solubility of the poly(meth)acrylamides will be increased when the pendent orthoester groups are acid-catalytically hydrolyzed. P*t*NiPM is not soluble in water at 37 °C because of its low CP (11.5 °C). Thus, the pH-dependent hydrolysis of P*t*NiPM was first studied by monitoring the turbidity changes of the polymer solutions with different pH at 37 °C (Figure S17). It is seen that the turbid solutions became transparent at specific times, meaning that the polymers were dissolved due to the partial hydrolysis of the orthoester groups. The time for the polymer solutions to become clear was prolonged with the increase of pH.

The ^{1}H NMR technique was further applied to qualitatively clarify the effects of R^3 and stereochemical structure on the acid-triggered hydrolysis behaviors of the polymers, including hydrolysis rate and the products. The measurements were performed in deuterated acetate buffer (pD 5.0) at 37 °C, and the ^{1}H NMR spectra as a function

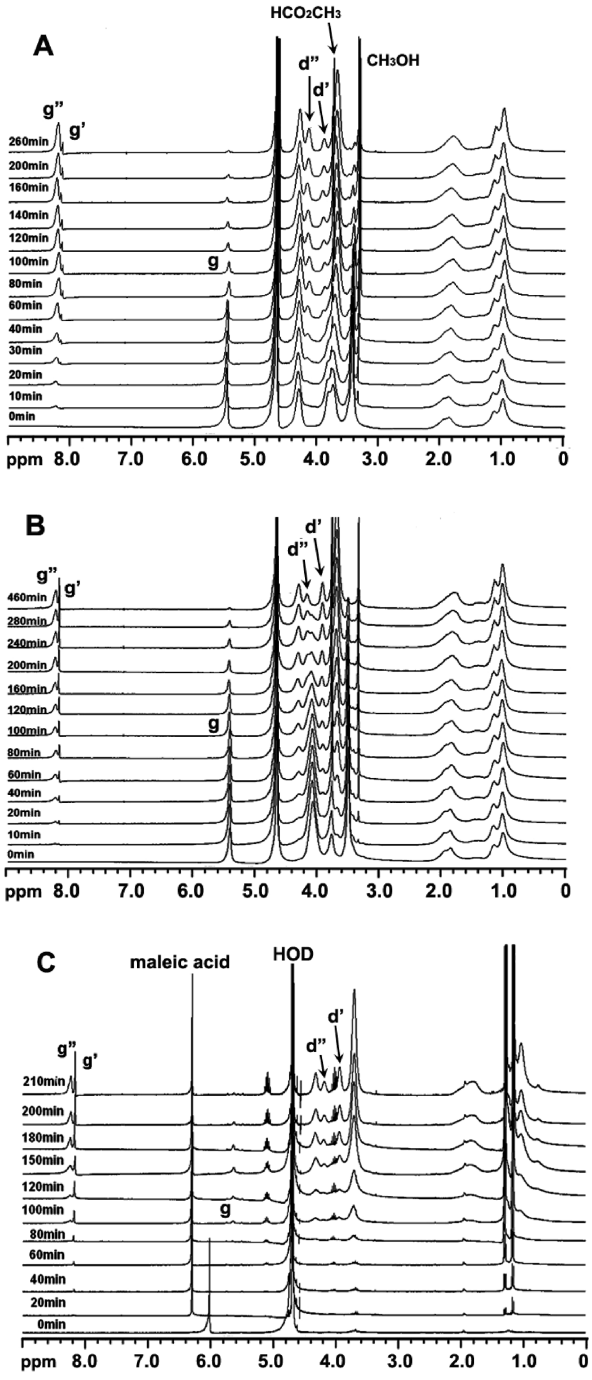

Figure 10. ^{1}H NMR spectra of P*c*NMM (A), P*t*NMM (B), and P*t*NiPM (C) in the deuterated acetate buffer at different hydrolysis times. pD 5.0, 37 °C.

of time are shown in Figure 10. All the proton signals of P*t*NMM and P*c*NMM were clearly observable at the starting point because the CPs of these two polymers were higher than 37 °C. The peak intensity of the orthoester methine proton (g) decreased gradually with the hydrolysis time and almost disappeared at 260 min for P*t*NMM and 400 min for P*c*NMM, respectively, indicating a faster hydrolysis rate of P*t*NMM as compared to that of P*c*NMM (Figure S18). The same trend was also observed for P*t*NEM and P*c*NEM (Figure S19).[8b] Acid-catalyzed hydrolyses of the monomers were also carried out at 37 °C in a homogeneous solution (Figures S20−S24). The results showed that the monomers with *trans* configuration also hydrolyzed

Scheme 2

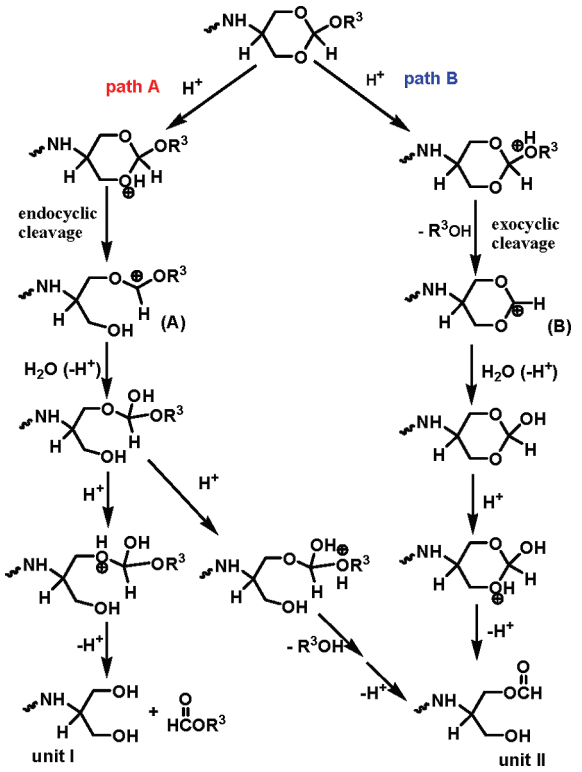

Scheme 3

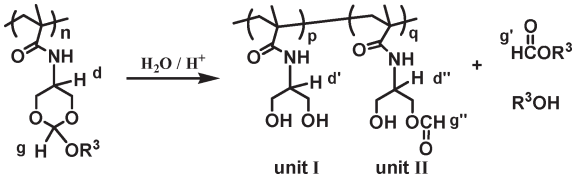

faster than those with *cis* configuration (Figures S25 and S26). In the case of P*t*NiPM, only very weak proton signals were observed at the starting point due to its low CP (< 37 °C). This polymer was gradually dissolved with prolonging the incubation time and hydrolyzed completely after 210 min. Regarding the effect of R^3, it is found that for an identical configuration the hydrolysis rate of the polymers increased as R^3 changed from methyl to isopropyl (Figure 10 and Figure S19). For the monomers, the same trend was obtained. The hydrolysis rate of the monomers follow the order of *trans*-NiPM > *trans*-NEM > *trans*-NMM, and *cis*-NEM > *cis*-NMM (Figures S25 and S26). This is rational because an electron-donating R^3 would help to stabilize the intermediate carbonium ions and promote hydrolysis of the cyclic orthoesters (Scheme 2).

Furthermore, we found that hydrolysis products of the polymers were significantly influenced by R^3 and the stereochemical structure of the pendent cyclic ring. As we reported previously, there are two kinds of units in the polymer chains when the orthoester groups are completely hydrolyzed: unit I with two hydroxy groups and unit II with one hydroxy group and one formate group (Scheme 3).[8b] The signals of d′ and d″ in ^{1}H NMR spectra of the hydrolyzed polymers are assigned to unit I and unit II, respectively (Figure 10 and Figure S19). By comparing the intensities of peaks d′ and d″, we can estimate the ratio of these two units. It is seen that for polymers with identical R^3 the ratio of unit I

to unit II increased as the configuration of the pendent cyclic orthoester structure changed from *trans* to *cis*. In other word, *cis* structure favors the formation of unit I. For the polymers with identical configuration, the ratio of unit I to unit II significantly increased when R^3 changed from methyl to ethyl and to isopropyl. In the case of acid-triggered hydrolysis of the monomers, we can observe the same trend by comparing the vinyl proton signals (a′ and a″ in Scheme S1 and Figures S20−S24). As shown in Scheme 2, hydrolysis of the cyclic orthoester proceeds mainly through two competing paths: the endocyclic ring cleavage (path A) and the breaking of the exocyclic alkyloxy group (path B).[8b,20] Path A results in the formation of both unit I and unit II while in path B only unit II can be obtained. The present ^{1}H NMR results demonstrated that path A became more important as R^3 changed from methyl to ethyl and to isopropyl whose electron-donating capability gradually increased. This can be explained rationally by the stability of the intermediate carbonium ion A. R^3 with more electron-donating capability is expected to have a stronger effect on stabilizing carbonium ion A but shows little effect on carbonium ion B (Scheme 2).

Conclusion

A family of poly(meth)acrylamide derivatives with pendent orthoester groups have been prepared. All the studied polymers except P*t*NPM are thermosensitive and susceptible to hydrolysis in mildly acidic media. The polymer structures, such as alkyl substitutes in the backbone and pendent moieties, and the stereochemical structure of the pendent cyclic orthoesters, exert significant effects on their aqueous solution properties including thermally induced phase transition/separation and acid-triggered hydrolysis. CPs of the polymers decrease with increasing the hydrophobicity of R^3 as well as changing the configuration from *cis* to *trans*. Polymers with a larger R^3 and *trans* configuration have a greater magnitude of dehydration and tend to exhibit a liquid−solid phase transition, while those with a smaller R^3 and *cis* configuration show a liquid−liquid phase separation with a smaller magnitude of dehydration. The polymers undergo an acid-triggered hydrolysis. Both R^3 and the stereochemical structure drastically influence the hydrolysis rate and products of the pendent orthoester groups in a combined fashion. In addition, the formation of colloidal loose aggregates formed below the LCSTs is a common feature for these poly(meth)acrylamides with the pendent cyclic orthoester moieties.

Acknowledgment. This work was financially supported by the National Natural Science Foundation of China (No. 20534010 and 50673004).

Supporting Information Available: NMR spectra of the monomers and polymers and their hydrolysis products, micrographs, more transmittance vs temperature plots, I_{338}/I_{333} vs polymer concentration plots, and hydrolysis kinetics. This material is available free of charge via the Internet at http://pubs.acs.org.

References and Notes

(1) (a) Gil, E. S.; Hudson, S. A. *Prog. Polym. Sci.* **2004**, *29*, 1173–1222. (b) Rijcken, C. J. F.; Soga, O.; Hennink, W. E.; van Nostrum, C. F. *J. Controlled Release* **2007**, *120*, 131–148. (c) Oh, K. T.; Yin, H. Q.; Lee, E. S.; Bae, Y. H. *J. Mater. Chem.* **2007**, *17*, 3987–4001. (d) Ganta, S.; Devalapally, H.; Shahiwala, A.; Amiji, M. *J. Controlled Release* **2008**, *126*, 187–204.

(2) (a) Dimitrov, I.; Trzebicka, B.; Muller, A. H. E.; Dworak, A. J.; Tsvetanov, C. B. *Prog. Polym. Sci.* **2007**, *32*, 1275–1343. (b) Yamato, M.; Akiyama, Y.; Kobayashi, J.; Yang, J.; Kikuchi, A.; Okano, T. *Prog. Polym. Sci.* **2007**, *32*, 1123–1133.

(3) (a) Schild, H. G. *Prog. Polym. Sci.* **1992**, *17*, 163–249. (b) Heskins, M.; Guillet, J. E. *J. Macromol. Sci., Chem.* **1968**, *A2*, 1441–1455. (c) Suwa, K.; Morishita, K.; Kishida, A.; Akashi, M. *J. Polym. Sci., Part A: Polym. Chem.* **1997**, *35*, 3087–3094.

(4) (a) Sugihara, S.; Hashimoto, K.; Okabe, S.; Shibayama, M.; Kanaoka, S.; Aoshima, S. *Macromolecules* **2004**, *37*, 336–343. (b) Han, S.; Hagiwara, M.; Ishizone, T. *Macromolecules* **2003**, *36*, 8312–8319. (c) Lutz, J. F. *J. Polym. Sci., Part A: Polym. Chem.* **2008**, *46*, 3459–3470.

(5) (a) Park, J. S.; Kataoka, K. *Macromolecules* **2006**, *39*, 6622–6630. (b) Feil, H.; Bae, Y. H.; Feijen, J.; Kim, S. W. *Macromolecules* **1993**, *26*, 2496–2500.

(6) (a) Huang, X. N.; Du, F. S.; Zhang, B.; Zhao, J. Y.; Li, Z. C. *J. Polym. Sci., Part A: Polym. Chem.* **2008**, *46*, 4332–4343. (b) Xia, Y.; Burke, N. A. D.; Stover, H. D. H. *Macromolecules* **2006**, *39*, 2275–2283. (c) Nakayama, M.; Okano, T. *Biomacromolecules* **2005**, *6*, 2320–2327. (d) Duan, Q.; Miura, Y.; Narumi, A.; Shen, X. D.; Sato, S.; Satoh, T.; Kakuchi, T. *J. Polym. Sci., Part A: Polym. Chem.* **2006**, *44*, 1117–1124. (e) Jiang, X. G.; Zhao, B. *J. Polym. Sci., Part A: Polym. Chem.* **2007**, *45*, 3707–3721.

(7) (a) Tang, Y. C.; Ding, Y. W.; Zhang, G. Z. *J. Phys. Chem. B* **2008**, *112*, 8447–8451. (b) Djokpe, E.; Vogt, W. *Macromol. Phys. Chem.* **2001**, *202*, 750–757. (c) Fujishige, S.; Kubota, K.; Ando, I. *J. Phys. Chem.* **1989**, *93*, 3311–3313.

(8) (a) Huang, X. N.; Du, F. S.; Ju, R.; Li, Z. C. *Macromol. Rapid Commun.* **2007**, *28*, 597–603. (b) Huang, X. N.; Du, F. S.; Liang, D. H.; Lin, S. S.; Li, Z. C. *Macromolecules* **2008**, *41*, 5433–5440. (c) Hruby, M.; Kucka, J.; Lebeda, O.; Mackova, H.; Babic, M.; Konak, C.; Studenovsky, M.; Sikora, A.; Kozempel, J.; Ulbrich, K. *J. Controlled Release* **2007**, *119*, 25–33. (d) Morinaga, H.; Morikawa, H.; Wang, Y. M.; Sudo, A.; Endo, T. *Macromolecules* **2009**, *42*, 2229–2235.

(9) Tang, R. P.; Palumbo, R. N.; Ji, W. H.; Wang, C. *Biomacromolecules* **2009**, *10*, 722–727.

(10) Stempel, G. H.; Cross, R. P.; Mariella, R. P. *J. Am. Chem. Soc.* **1950**, *72*, 2299–2300.

(11) Huang, X. N.; Du, F. S.; Cheng, J.; Dong, Y. Q.; Liang, D. H.; Ji, S. P.; Lin, S. S.; Li, Z. C. *Macromolecules* **2009**, *42*, 783–790.

(12) (a) Kalyanasundaram, K.; Thomas, J. K. *J. Am. Chem. Soc.* **1977**, *99*, 2039–2044. (b) Wilhelm, M.; Zhao, C. L.; Wang, Y. C.; Xu, R. L.; Winnik, M. A.; Mura, J. L.; Riess, G.; Croucher, M. D. *Macromolecules* **1991**, *24*, 1033–1040. (c) Winnik, F. M. *Chem. Rev.* **1993**, *93*, 587–614.

(13) (a) Aathimanikandan, S. V.; Savariar, E. N.; Thayumanavan, S. *J. Am. Chem. Soc.* **2005**, *127*, 14922–14929. (b) Lee, E. S.; Oh, K. T.; Kim, D.; Youn, Y. S.; Bae, Y. H. *J. Controlled Release* **2007**, *123*, 19–26.

(14) (a) Cheng, H.; Shen, L.; Wu, C. *Macromolecules* **2006**, *39*, 2325–2329. (b) Ding, Y. W.; Ye, X. D.; Zhang, G. Z. *Macromolecules* **2005**, *38*, 904–908. (c) Maeda, Y.; Nakamura, T.; Ikeda, I. *Macromolecules* **2001**, *34*, 8246–8251.

(15) Keerl, M.; Smirnovas, V.; Winter, R.; Richtering, W. *Angew. Chem., Int. Ed.* **2008**, *47*, 338–341.

(16) (a) Tiktopulo, E. I.; Uversky, V. N.; Lushchik, V. B.; Klenin, S. I.; Bychkova, V. E.; Ptitsyn, O. B. *Macromolecules* **1995**, *28*, 7519–7524. (b) Kubota, K.; Hamano, K.; Kuwahara, N.; Fujishige, S.; Ando, I. *Polym. J.* **1990**, *22*, 1051–1057. (c) Ito, S. *Kobunshi Ronbunshu* **1989**, *46*, 437–443.

(17) (a) Yin, X. C.; Stover, H. D. H. *Macromolecules* **2005**, *38*, 2109–2115. (b) Maeda, T.; Kanda, T.; Yonekura, Y.; Yamamoto, K.; Aoyagi, T. *Biomacromolecules* **2006**, *7*, 545–549. (c) Yamamoto, K.; Serizawa, T.; Akashi, M. *Macromol. Chem. Phys.* **2003**, *204*, 1027–1033. (d) Yamaoka, T.; Tamura, T.; Seto, Y.; Tada, T.; Kunugi, S.; Tirrell, D. A. *Biomacromolecules* **2003**, *4*, 1680–1685.

(18) (a) Chung, J. E.; Yokoyama, M.; Suzuki, K.; Aoyagi, T.; Sakurai, Y.; Okano, T. *Colloids Surf., B* **1997**, *9*, 37–48. (b) Schild, H. G.; Tirrell, D. A. *Langmuir* **1991**, *7*, 1319–1324. (c) Gao, Z. Q.; Liu, W. G.; Gao, P.; Yao, K. D.; Li, H. X.; Wang, G. H. *Polymer* **2005**, *46*, 5268–5277.

(19) (a) Arotcarena, M.; Heise, B.; Ishaya, S.; Laschewsky, A. *J. Am. Chem. Soc.* **2002**, *124*, 3787–3793. (b) Weaver, J. V. M.; Armes, S. P.; Butun, V. *Chem. Commun.* **2002**, 2122–2123. (c) Maeda, Y.; Mochiduki, H.; Ikeda, I. *Macromol. Rapid Commun.* **2004**, *25*, 1330–1334. (d) Chang, Y.; Chen, W. Y.; Yandi, W.; Shih, Y. J.; Chu, W. L.; Liu, Y. L.; Chu, C. W.; Ruaan, R. C.; Higuchi, A. *Biomacromolecules* **2009**, *10*, 2092–2100. (e) Sugihara, S.; Kanaoka, S.; Aoshima, S. *J. Polym. Sci., Part A: Polym. Chem.* **2004**, *42*,

2601–2611. (f) Li, C.; Buurma, N. J.; Haq, I.; Turner, C.; Armes, S. P.; Castelletto, V.; Hamley, I. W.; Lewis, A. L. *Langmuir* **2005**, *21*, 11026–11033. (g) Mertoglu, M.; Garnier, S.; Laschewsky, A.; Skrabania, K.; Storsberg, J. *Polymer* **2005**, *46*, 7726–7740. (h) Hua, F. J.; Jiang, X. G.; Zhao, B. *Macromolecules* **2006**, *39*, 3476–3479. (i) Cao, Y.; Zhao, N.; Wu, K.; Zhu, X. X. *Langmuir* **2009**, *25*, 1699–1704. (j) Shan, J.; Chen, J.; Nuopponen, M.; Tenhu, H. *Langmuir* **2004**, *20*, 4671–4676. (k) Luo, S. Z.; Xu, J.; Zhu, Z. Y.; Wu, C.; Liu, S. Y. *J. Phys. Chem. B* **2009**, *110*, 9132–9139.

(20) (a) Ahmad, M.; Bergstrom, R. G.; Cashen, M. J.; Chiang, Y.; Kresge, A. J.; McClelland, R. A.; Powell, M. F. *J. Am. Chem. Soc.* **1979**, *101*, 2669–2677. (b) Li, S. G.; Dory, Y. L.; Deslongchamps, P. *Tetrahedron* **1996**, *52*, 14841–14854. (c) By, K.; Nantz, M. H. *Angew. Chem., Int. Ed.* **2004**, *43*, 1117–1120.